Supplementary Information

Omar Mokhtari, Michel Quintard, Yohan Davit

Mesh convergence

A detailed study of the mesh convergence properties of our scheme is given in Mokhtari *et al.* (2023) for the lid-driven cavity and flow past a single cylinder. An additional convergence study in the case of a single cylinder is also given in Mokhtari *et al.* (2022), with a more detailed analysis of average properties such as the drag coefficient. Here, we provide an example of mesh convergence on a hexagonal lattice of cylinders in the aligned configuration, a case specific to the work in this paper. Our goal is to illustrate how mesh size influences result.

To assess convergence, we consider the evolution of the angle α with the size of the mesh, fixing the angle $\theta = 15^\circ$ and progressively increasing the Weissenberg number, starting from $Wi = 0$. The geometry consists of 30 cylinders in the aligned configuration. Periodic boundary conditions are applied to the pairs constituted by the left/right and top/bottom sides. The structured uniform mesh is obtained by cutting each side of the domain into N equal parts and excluding each cell whose centre $(x_K, y_K)^\mathsf{T}$ verifies

$$\min_{C \in \{\text{cylinders}\}} \sqrt{(x_K - x_C)^2 + (y_K - y_C)^2} \leq R, \tag{1}$$

where $(x_C, y_C)^\mathsf{T}$ is the centre of a cylinder C and R the radius. This mesh can then be refined by splitting each side into r equal parts and thus by splitting each cell into $r \times r$ parts, see Fig 1. We thus consider two approaches to convergence. The first one consists in varying N with r given, thus improving both the details of the geometry and the mesh in the bulk of the fluid. The second one consists in fixing N, thus fixing the geometry, and varying r to improve mesh quality in the fluid. We observe an excellent convergence of the flow angle with mesh refinement, even for relatively large Weissenberg numbers, Fig 2. Even though the exact value of the flow angle slightly depends on the mesh size, we always correctly describe the stickiness of the strands with closest neighbors.

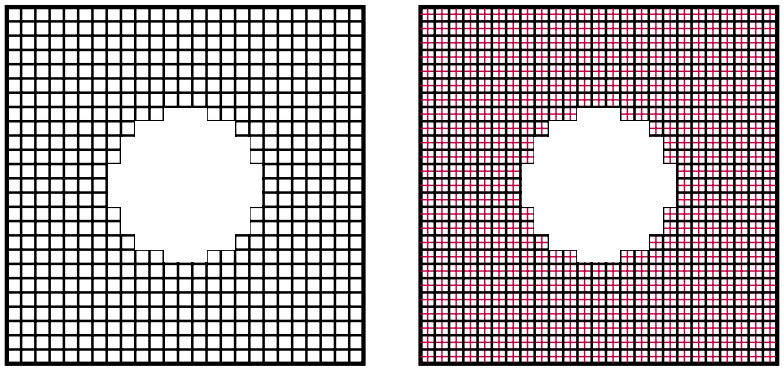

(**a**) "Stair-steps" ($N = 25$) (**b**) Refinement ($r = 2$)

Figure 1: Mesh and refinement. (**a**) Example of mesh around a single circle in the case $N = 25$. (**b**) Refinement in the case $r = 2$ showing in red how each cell is cut in 4.

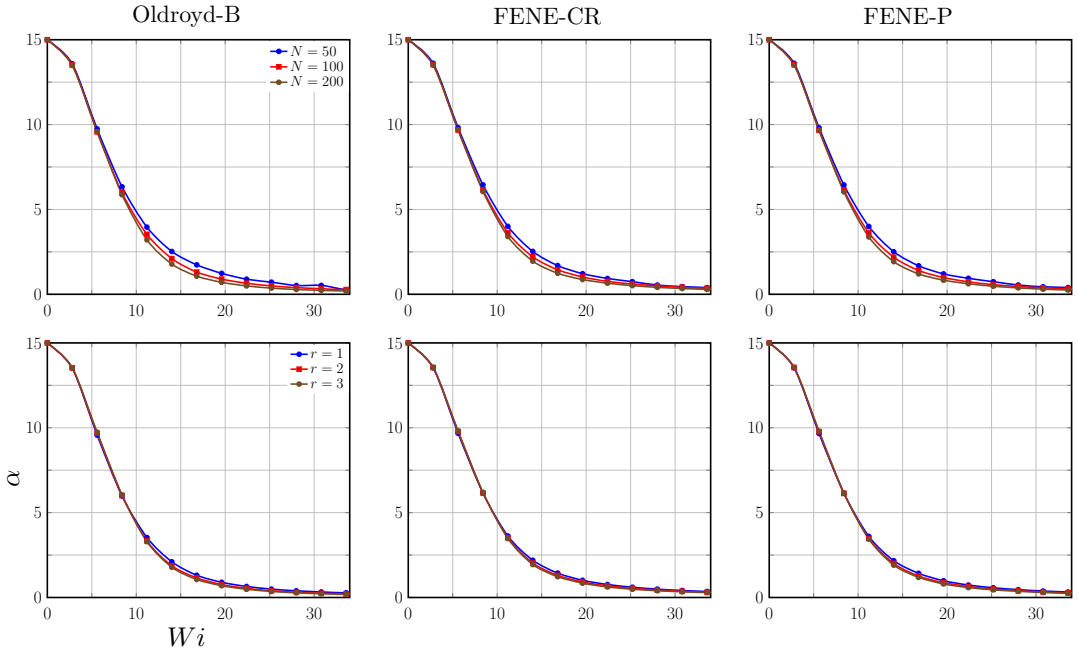

Figure 2: Convergence analysis for steady viscoelastic flow through a hexagonal lattice of circles. Plots of the angle α as a function of Wi for $\beta = 1$ in the case $\theta = 15^\circ$ and the FENE-P, FENE-CR and Oldroyd-B models. Each curve is obtained by fixing the angle θ and progressively increasing Wi, starting from $Wi = 0$. The first line compares the results for different values of the mesh size N with a fixed value of the mesh refinement $r = 1$. The second line compares different values of the mesh refinement r with a fixed mesh size $N = 100$.

Supplementary figures

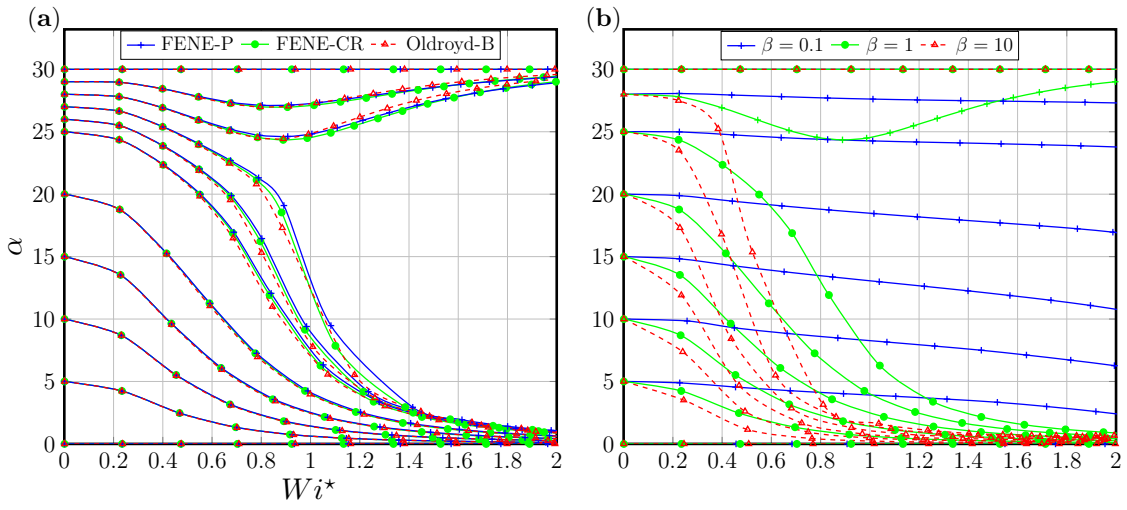

Figure 3: Same as Figure 3 in the article but with a different definition of the Wi number. Here we have used $Wi = \lambda\langle\|\mathbf{u}\|\rangle/H$ with $\langle\cdot\rangle = 1/|\Omega| \int_\Omega \cdot\, d\Omega$ and Ω the fluid domain, which corresponds to a more common definition of the Wi number. (**a**) Plots of the angle α between the direction of the average flow velocity and $\mathbf{x}$ as a function of the Weissenberg number, Wi, for the viscosity ratio $\beta = 1$, different values of θ, and the FENE-P, FENE-CR and Oldroyd-B models. Each curve is obtained by fixing the angle θ and progressively increasing Wi, starting from $Wi = 0$. At $Wi = 0$, the flow is Newtonian so that the average flow velocity is along the direction of the forcing term and the value of θ for each curve can be determined as $\theta = \alpha\,(Wi = 0)$. (**b**) Plots of the angle α as a function of Wi for the Oldroyd-B model and different values of θ and β. In both (**a**) and (**b**): points are actual computations and lines are just guides for the eyes; graphs are limited to the range $\theta \in [0, 30^\circ]$ because of the 6-fold rotational symmetry combined with the reflection symmetry about the $\mathbf{x}$ axis.

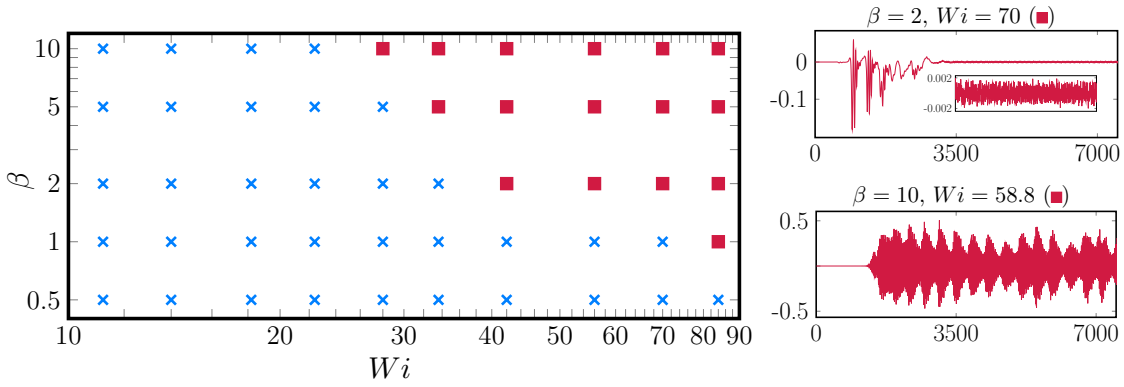

Figure 4: Diagram of the different regimes obtained for the FENE-CR model with $b = 1000$ (Methods) in the aligned configuration. The main graph shows the different regimes as a function of β and Wi. (×) corresponds to the trivial steady solution and (■) to the pulsating regime. The other plots are examples of time evolutions of α for the regime (**V**).

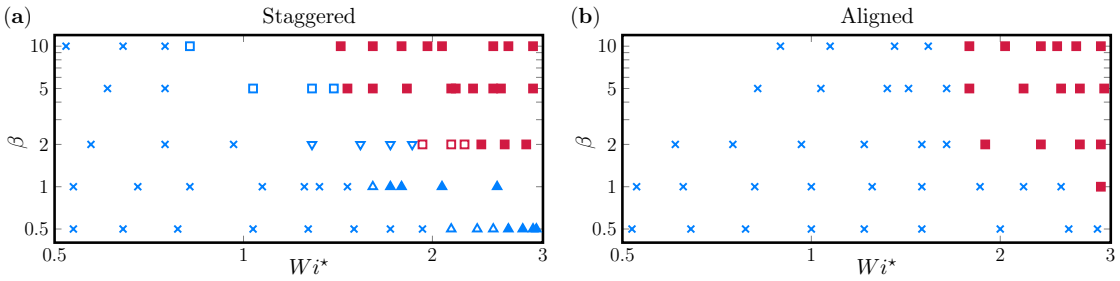

Figure 5: (**a**) Same as Figure 11 in the article and (**b**) same as Figure 4 in the Supplementary Information, with a different definition of the Wi number. Here we have used $Wi = \lambda \langle \|\mathbf{u}\| \rangle / H$ with $\langle \cdot \rangle = 1/|\Omega| \int_\Omega \cdot \, d\Omega$ and Ω the fluid domain, which corresponds to a more common definition of the Wi number.

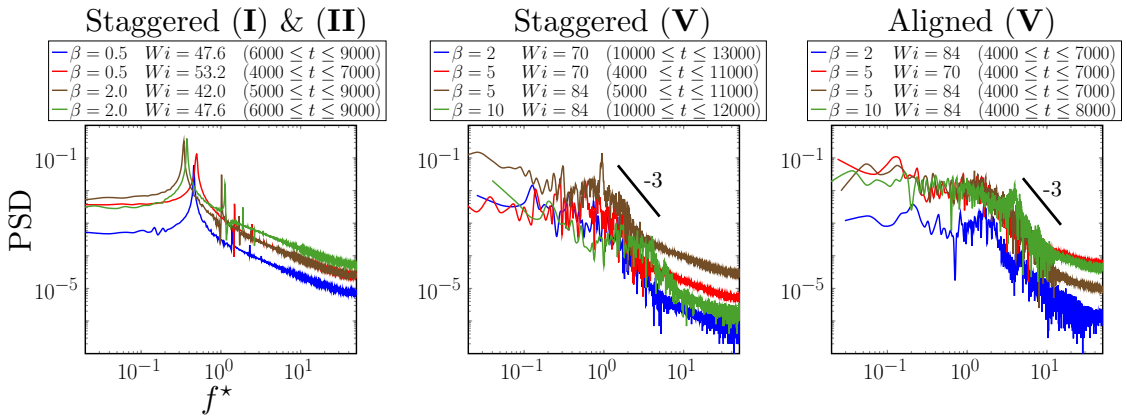

Figure 6: Same as Figure 12 in the article but with a different definition of the dimensionless frequency. Here, we have used $f^\star = Wi \times f$, which corresponds to a non-dimensionalization of time with the characteristic time for polymer relaxation, λ.

Supplementary videos

Movie 1 Evolution of the flow angle, alpha, as a function of the Weissenberg number for a fixed value of the force angle, theta (Oldroyd-B model, theta=25 degrees).

The field in color (log scale) is the trace of the conformation tensor and shows the position of the birefringent strands in red. This movie illustrates the stickiness of the strands with the closest neighbor at angle 0.

Movie 2 Hysteresis of the flow angle, alpha, with the force angle, theta (Oldroyd-B model, Wi=24).

The figure on the right is the plot of alpha as a function of theta. The figure on the right in color (log scale) is the trace of the conformation tensor and shows the position of the birefringent strands in red. The movie follows hysteretic loops with a red point indicating the trajectories and shows the corresponding fields for the trace of the conformation tensor—with stickiness at 0 and 60 degrees.

Movie 3 Simulation of a viscoelastic flow in a staggered array of cylinders (FENE-CR model, b=1000, Beta=0.5 and Wi=47.6).

On the left, we plot the trace of the conformation tensor (log scale). On the right, we plot the corresponding normalized velocity field. This movie illustrates regime (I) with self-sustained oscillations.

Movie 4 Simulation of a viscoelastic flow in a staggered array of cylinders (FENE-CR model, b=1000, Beta=2 and Wi=47.6).

On the left, we plot the trace of the conformation tensor (log scale). On the right, we plot the corresponding normalized velocity field. This movie illustrates regime (II) with travelling waves.

Movie 5 Simulation of a viscoelastic flow in a staggered array of cylinders (FENE-CR model, b=1000, Beta=5 and Wi=58.8).

On the left, we plot the trace of the conformation tensor (log scale). On the right, we plot the corresponding normalized velocity field. This movie illustrates regime (V) with pulsations.

Movie 6-a Simulation of a viscoelastic flow in a staggered array of cylinders (FENE-CR model, b=1000, Beta=10 and Wi=84).

On the left, we plot the trace of the conformation tensor (log scale). On the right, we plot the corresponding normalized velocity field. This movie illustrates transient defects.

Movie 6-b Simulation of a viscoelastic flow in a staggered array of cylinders (FENE-CR model, b=1000, Beta=10 and Wi=84).

On the left, we plot the trace of the conformation tensor (log scale). On the right, we plot the corresponding normalized velocity field. This movie illustrates the disappearance of defects and the transition to regime (V) with pulsations.

References

MOKHTARI, O., DAVIT, Y., LATCHÉ, J.-C. & QUINTARD, M. 2023 A staggered projection scheme for viscoelastic flows. *Mathematical Modelling and Numerical Analysis (ESAIM: M2AN)* **57** (3), 1747–1793.

MOKHTARI, O., LATCHÉ, J.-C., QUINTARD, M. & DAVIT, Y. 2022 Birefringent strands drive the flow of viscoelastic fluids past obstacles. *Journal of Fluid Mechanics* **948**, A2.